HHS Public Access

Author manuscript

Biomacromolecules. Author manuscript; available in PMC 2020 August 21.

Published in final edited form as:

Biomacromolecules. 2016 July 11; 17(7): 2459–2465. doi:10.1021/acs.biomac.6b00597.

Oxygen-Purged Microfluidic Device to Enhance Cell Viability in Photopolymerized PEG Hydrogel Microparticles

Bingzhao Xia, **Kaspars Krutkramelis**, **John Oakey***

Department of Chemical Engineering, University of Wyoming, Laramie, Wyoming 82071, United States

Abstract

Encapsulating cells within biocompatible materials is a widely used strategy for cell delivery and tissue engineering. While cells are commonly suspended within bulk hydrogel-forming solutions during gelation, substantial interest in the microfluidic fabrication of miniaturized cell encapsulation vehicles has more recently emerged. Here, we utilize multiphase microfluidics to encapsulate cells within photopolymerized picoliter-volume water-in-oil droplets at high production rates. The photoinitiated polymerization of polyethylene glycol diacrylate (PEGDA) is used to continuously produce solid particles from aqueous liquid drops containing cells and hydrogel forming solution. It is well understood that this photoinitiated addition reaction is inhibited by oxygen. In contrast to bulk polymerization in which ambient oxygen is rapidly and harmlessly consumed, allowing the polymerization reaction to proceed, photopolymerization within air permeable polydimethylsiloxane (PDMS) microfluidic devices allows oxygen to be replenished by diffusion as it is depleted. This sustained presence of oxygen and the consequential accumulation of peroxy radicals produce a dramatic effect upon both droplet polymerization and post-encapsulation cell viability. In this work we employ a nitrogen microjacketed microfluidic device to purge oxygen from flowing fluids during photopolymerization. By increasing the purging nitrogen pressure, oxygen concentration was attenuated, and increased post-encapsulation cell viability was achieved. A reaction-diffusion model was used to predict the cumulative intradroplet concentration of peroxy radicals, which corresponded directly to post-encapsulation cell viability. The nitrogen-jacketed microfluidic device presented here allows the droplet oxygen concentration to be finely tuned during cell encapsulation, leading to high post-encapsulation cell viability.

Graphical Abstract

***Corresponding Author:** joakey@uwyo.edu.

The authors declare no competing financial interest.

ASSOCIATED CONTENT

Supporting Information

The Supporting Information is available free of charge on the ACS Publications website at DOI: 10.1021/acs.bio-mac.6b00597.

Reaction-diffusion model details: PEG-DA photopolymerization reaction steps and physical and kinetic constants (PDF).

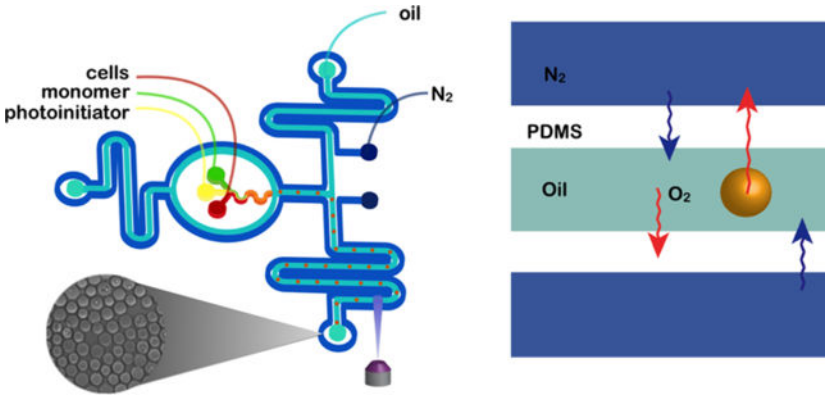

1. INTRODUCTION

Encapsulating cells within tissue-like semipermeable hydrogels can impart protection from mechanical stress and the host immune system, while allowing bidirectional diffusion of nutrients and wastes.[1,2] Immobilizing cells within hydrogel scaffolds can therefore facilitate cell product delivery over long time periods, locate reparative cells at injury sites, and enable the potential for therapeutic transplantation of nonhuman cells. Stem cells, for instance, possess vast potential for tissue engineering applications and cell encapsulation technology will be necessary to provide permissive niches, guide differentiation and development, and prevent deleterious immune responses.[3] Over the past two decades, cell encapsulation has been studied and developed as a potential therapy for type 1 diabetes,[4] bone regeneration,[5,6] cartilage formation,[7] and vascular differentiation.[8] A host of natural and synthetic polymer hydrogels have been utilized for encapsulation,[4,8–10] including PEG-based hydrogels, which are particularly versatile due to their excellent biocompatibility, tunable network structure, and readily modified properties.[11] The photoinitiated gelation of PEG-based macromers has significantly expanded potential application as cells can now be encapsulated under physiological conditions with precise control over temporal and spatial properties.[12]

More recently, the miniaturization of hydrogels by microfabrication and microfluidic technologies[13] has emerged as an area of intense research interest with broad utility in biosensing,[14] materials synthesis,[15,16] and therapeutics.[17] Micropatterned hydrogels have also been used to study fundamental cell behavior, such as adhesion and motility.[18,19] Encapsulating cells within microstructured hydrogels may provide a mesoscale link between macromolecular and macroscopic length scales[20,21] and can offer many benefits including controlled cell distribution, tailored mechanical properties, and improved diffusive properties, critical to regulating cell function and maintaining viability.[22,23] Miniaturized encapsulation technologies have also been used to analyze cell productivity,[17] molecular uptake and cellular survival,[24] and cell–cell[25] and cell–matrix[26] interactions.

Several approaches have been explored for cell microencapsulation. Micromolding was first employed to generate shape-specific microgels that were subsequently self-assembled to generate tissue constructs.[27] Stop flow lithography (SFL) was employed to photoencapsulate cells within PEG hydrogel particles of arbitrary two-dimensional shape at improved rates.[28]

While compromised cell viability was reported following in situ photopatterning, these examples represent a compelling demonstration of the potential for cell encapsulation in microgels. An array of microfabrication techniques have also been used to pattern PEG hydrogels and the spatial distribution of functional molecules or mechanical properties. For instance, gradient hydrogels were generated to study the effects of RGDS concentration on encapsulated cells,[18,29] while oxygen gradients were exploited during SFL to form extremely elastic particles[30] and particles with cross-linking density gradients and patterned degradation profiles.[13] Interest in increasing the fabrication frequency of microscale hydrogels has brought attention to microfluidic emulsification, a method of forming surfactant-stabilized aqueous droplets in a continuous oil phase at intersecting microfluidic channels[31,32] or in coaxial capillaries.[33] This approach can produce highly monodisperse microdroplets at exceptionally high rates (~10 kHz), suggesting broad utility for high throughput cell compartmentalization and subsequent encapsulation via polymerization.[13] Indeed, single cells have been distributed into natural polymeric hydrogel particles,[34] as well as very large PEGDA particles.[26,35] As we demonstrate in this work, the lower size limit of these particles, as well as the viability of cells encapsulated via stop flow lithography, are constrained by the oxygen-inhibition of PEGDA photopolymerization.[36,37]

The ease of described techniques for microscale hydrogel molding and microparticle production has been largely enabled by the introduction of polydimethylsiloxane (PDMS)-based microfluidic devices.[38] PDMS devices, which have been widely adopted for use in bioengineering applications, can be quickly and inexpensively fabricated via replica molding from a photolithographically patterned master. Notably, PDMS is highly permeable to oxygen, which is generally an advantage for cell-incubation studies[39] and related research. Enabling to SFL, the oxygen flux from PDMS surfaces locally prohibits polymerization in the near wall region, but sustains the production of peroxy radicals generated during oxygen inhibition.[28] Thus, to obtain fully polymerized microgels, a higher photoinitiator concentration must be used, which presents its own harmful effects on cells, including, lipid peroxidation,[40] oxidation of amino acids,[41] inactive specific enzymes,[42–44] and damage of DNA.[45] The facilitated transport of oxygen to aqueous emulsion droplets flowing through PDMS channels is further assisted by the use of fluorinated oils, which possess extremely high oxygen solubilities.[46] Increasing particle size[35] improves cell viability during photopolymerization, but this approach restricts the minimum overall drop size and extent of drop polymerization. We have recently introduced a nitrogen-jacketed PDMS device that allows complete droplet photopolymerization by preventing ambient oxygen from diffusing into the system.[46] An alternative to oxygen purging is the use of oxygen-impermeable plastic or glass based devices, but initial results indicate cell viability to be poor following polymerization in these platforms. We hypothesize that poor cell viability is the result of residual oxygen that remains in the carrier phase and macromer solution.

To increase post-encapsulation cell viability, we introduce a nitrogen-jacketed microfluidic device in this work, which not only prevents ambient oxygen from diffusing into the system, but also purges residual oxygen from the carrier phase and macromer solution prior to droplet formation. Employing this new device, we have been able to locally control the oxygen concentration in the microfluidic system and demonstrate significantly improved viability of encapsulated cells. A finite element reaction-diffusion model was utilized to

predict the concentration of peroxy radicals generated and accumulated during photopolymerization, demonstrating that the post-encapsulation viability was linked to residual oxygen concentration.

2. EXPERIMENTAL SECTION

2.1. Cell Culture

Human lung adenocarcinoma epithelial cells (A549) were maintained in low-glucose Dulbecco's modified Eagles's medium (DMEM; Life Technologies, U.S.A.) supplemented with 10% fetal bovine serum (Life technologies, U.S.A.), 1% PenStrep, and 0.2% Fungizone (Sigma-Aldrich, U.S.A.). All cells were cultured in a 5% CO_2 humidified incubator at 37 °C.

2.2. Two-Layer PDMS Device Fabrication

Two-layer microfluidic devices were fabricated using soft lithography techniques.[47] Briefly, a silicon wafer (Silicon Inc., U.S.A.) was first patterned with SU-8 2015 negative photoresist (MicroChem, MA, U.S.A.) at a thickness of 30 μm. Features were polymerized by collimated UV light exposure (Omnicure S2000, U.S.A.) through a photomask (CAD/Art Services, OR) and removal of the uncured photoresist in developer (propylene glycol monomethyl ether acetate, Sigma-Aldrich, U.S.A.). A second planar flow network was patterned with SU-8 100 at thickness of 100 μm by the same method. Polydimethylsiloxane (PDMS, Dow Corning, MI) was cast upon the silicon wafer and the cured elastomer was removed, trimmed and punched with a sharpened 20G dispensing needle (Brico Medical Supplies, Inc., U.S.A.) to fashion inlet and outlet holes. Finished devices were created by bonding PDMS replicas to glass slides following oxygen plasma treatment. To ensure a hydrophobic surface for aqueous droplet generation, Aquapel (PPG Industries) was briefly injected into the device and flushed with nitrogen.

2.3. Hydrogel-Forming Polymer Solution

A549 cells were detached with 0.05% trypsin/ethylenediaminetetraacetic acid (Life-technologies, U.S.A.), pelleted, and resuspended at an effective cell density of 3×10^7 cells/mL in heavy phosphate-buffered saline (PBS), which was adjusted to have a specific gravity of 1.05 g/mL by OptiPrep density medium (Sigma-Aldrich, U.S.A.). The macromer mixture contained 75 mol % polyethylene glycol monoacrylate (PEGMA, $M_n \approx 400$ Da; monomer–polymer and Dajac Laboratories), and 25 mol % poly(ethylene glycol) diacrylate (PEGDA, $M_n \approx 3400$ Da; Alfa Aesar, MA),[48] and was diluted to a final mass fraction of 45 wt % macromer in phosphate buffered saline (PBS, pH 7.4, SigmaAldrich, U.S.A.). The photoinitiator lithium phenyl-2,4,6-trimethylbenzoylphosphinate (LAP) was synthesized as previously described[49] and dissolved in PBS. The hydrogel-forming polymer solution was mixed in a vial or within a microfluidic device to a final concentration of 15 total wt % monomer mixture, a final cell density of 1×10^7 cells/mL, and a LAP concentration ranging from 1 to 10 mg/mL.

2.4. Microfluidic Cell Encapsulation

For microfluidic encapsulation, the macromer mixture, cells suspension, and LAP were loaded into syringes and independently injected into the microfluidic device with a flow rate of 0.33 μL/min. Simultaneously, fluorocarbon oil (Novec 7500, containing 2 wt % Pico-Surf (Dolomite, U.S.A.)) was also injected into the device as an immiscible oil phase at 2 and 7 μL/ min for the first layer and second layer of the device, respectively. At the droplet-generating junction (Figure 3A) of the thinner layer of the device, the aqueous prepolymer precursor was sheared into 40 μm diameter droplets. Traveling to the thicker layer of the device, the droplet volume fraction was reduced and interparticle spacing maintained by the introduction of additional oil. Droplets passed through a serpentine channel where they were continuously polymerized by exposure to UV light (220 mW/cm^2, Mecury-100W, Chiu Technical Corporation, U.S.A.) for 0.35 s before exiting the device for collection. Microsphere hydrogels collected from the device were separated from oil by washing on a 5 μm cell strainer (VWR, U.S.A.) with PBS and 0.1 wt % Pluronic F-127 (Sigma-Aldrich, U.S.A.). Cell-laden particles were finally resuspended into cell culture medium with 0.1 wt % Pluronic F-127 and cultured in 24-well plates. All experiments were performed with quadruplicate wells for each condition.

2.5. Bulk Cell Encapsulation

PEGDA hydrogel-forming macromer solutions were prepared according to protocols described above. To achieve a bulk emulsion, 100 μL of the macromer solution was added to Novec 7500 with 2% Pico-surf or light Mineral Oil with 2% Span 80 (Sigma-Aldrich, U.S.A.), and vortexed at 1000 osc/min for 10 s to achieve a well-homogonized emulsion, which was polymerized by exposure to UV light for 2 s. Hydrogel particles were separated from the oil and washed using the protocols described above.

2.6. Cell Viability Assessment

Cells encapsulated in hydrogel microspheres were stained for viability after resuspension in PBS using a LIVE/DEAD Viability/Cytotoxicity Kit for mammalian cells (Life Technologies, U.S.A.; calcein AM at 2 μM, ethidium homodimer-1 at 4 μM). Live and dead cells were counted manually using an inverted fluorescence microscope IX-71 (Olympus, U.S.A.) and the corresponding cell viability was calculated relative to controls. Control cells had not been encapsulated, and they were separated from oil and washed on a 5 μm cell strainer (pluriSelect, U.S.A.) using PBS with 0.1 wt % Pluronic F-127. Viability of control cells was assayed using the method described above.

2.7. Photopolymerization Modeling

A reaction-diffusion model of free radical photopolymerization was constructed and used to quantify peroxy radical accumulation and establish their effect upon cell viability in photopolymerized hydrogel microparticles, where the peroxy radicals were assumed inert after produced. The exposure time used in this step (0.35 s) was calculated based on the total flow rate of the fluid and the geometry of the microfluidic device. A finite element numerical model was created in the COMSOL multiphysics software package using parameters and settings outlined below. A line drawn in 1-D axisymmetric space was set to

represent a distance from droplet center to the droplet interface. A time-dependent transport of diluted species study was selected across the line as the model basis using the characteristic mass transport equation as follows:

$$\frac{\partial c_i}{\partial t} + \nabla \cdot (-\nabla c_i) = R_i$$
$$N_i = -D_i \nabla c_i$$

In the droplet photopolymerization model, the reacting species were: macromer, initiator, free radicals, and oxygen. The full, detailed reaction sequence has been previously described.[46] Briefly, initiator species are converted into free radicals during the first polymerization step, initiator photolysis. Next, free radical species are allowed to react along three different pathways: (1) monomer chain initiation/propagation, (2) radical self-termination, and (3) radical termination with oxygen leading to the peroxy radical formation. Additionally, oxygen is allowed to freely diffuse into the droplet, and react with free initiator and macromere radicals. All reaction parameters used in this model were obtained from the literature.[49–54] Based upon experimental observations of nitrogen jacket effectiveness, an assumption was made that the oxygen concentration in a droplet within a purged microchannel was dilute. The pressure-dependent oxygen concentration, 0.01 mol/m^3, was calculated using the data in this experiment and our reaction diffusion model.[46]

3. RESULTS AND DISCUSSION

3.1. Size Distribution and Uniformity of Microsphere Hydrogels

All cell encapsulation experiments were conducted in either bulk (Figure 1A) or completely within a microfluidic device (Figure 1B) using mineral oil +2% Span 80 or Novec 7500 + 2% Pico-Surf as the immiscible carrier phase, and with 1 wt % LAP as the photoinitiator in the aqueous phase. Microsphere hydrogels were collected and resuspended into PBS by vortexing with 0.1% Pluronic F-127 in PBS. The device depth was 30 μm, which was chosen to generate droplets with a diameter less than 50 μm. Hydrogel particles were imaged using bright field microscopy and their diameters were measured using ImageJ. Uniformity, a measure of particle size polydisipersity,[55] and size distributions in terms of number are shown in Figure 1C and D, respectively. These results confirm previously documented experiments, in which microfluidic devices were shown to produce emulsion droplets and microparticles with much tighter size distributions than those produced by bulk emulsification. We also illustrate that, in comparison with mineral oil, employing Novec oil provides better control of particle size with an improvement in monodispersity using the identical device and flow rate conditions. These results clearly describe the advantages of utilizing, not only a microfluidic approach for droplet generation, but a fluorocarbon oil over a hydrocarbon oil. With control of droplet and particle size and uniformity, one can also readily achieve delicate control over deterministic cell encapsulation processes.[56,57]

3.2. Hydrogel Solution Formulation Composition Effect on Post-Encapsulation Cell Viability

Encapsulating cells within microfabricated biocompatible hydrogels is a promising strategy for cell delivery and tissue engineering. There are various methods to generate cell-laden microgels, such as via bulk emulsification[58] or with microfluidic devices[59]using different immiscible oil carrier phases. We compared these two methods with two different oils, mineral oil and Novec 7500 to conduct cell encapsulation within microgel particles. While Novec 7500 produces microgels with excellent control over particle size and uniformity, the post-encapsulation cell viability was effectively zero for both bulk and microfluidic processing (Figure 2A).

To explore the complete loss of cell viability when conducting cell encapsulation and photopolymerization with Novec 7500, a series of control experiments was conducted using mineral oil and Novec oil in PDMS microfluidic devices. Individual components were added to the aqueous solution and UV light exposure was increased in a stepwise manner in order to evaluate the toxicity of each element and combination of elements. The results of these systematic experiments reveal that only encapsulation and polymerization in Novec 7500, in the presence of initiator and UV exposure, produced the observed collapse in post-encapsulation cell viability (Figure 2B). Although both oils used are biocompatible, they possess vastly different oxygen solubilities at room temperature; perfluorinated oils have a much higher oxygen solubility (5.0 mol/m[360]) than mineral oil (1.02 mol/m[361]). Oxygen is well-known as an inhibitor of free radical chain polymerization. During this inhibitory side reaction, photoinitiator radicals are scavenged by oxygen to produce ROS, which in turn are deleterious to cells by reacting with lipids, amino acids, and proteins.[28,62] This effect is compounded when photopolymerization is conducted in PDMS devices in which the oil is in direct contact with the elastomer walls. The excellent gas and oxygen permeability of PDMS[63,64] allows consumed oxygen to be quickly replenished and the oxygen concentration of the oil to be maintained at its saturation level. Based on our initial observations, we hypothesize that this rapid oxygen replenishment leads directly to an amplified accumulation of peroxy radicals during the course of photopolymerization, with profoundly harmful effect to the post-encapsulation cell viability.

3.3. Oxygen Controllable Microfluidic System for Cell Encapsulation

As the generation of deleterious ROS species arises from the conversion of oxygen to peroxy radicals during the photoinitiated PEGDA polymerization reaction, it is important to establish a quantitative measure of oxygen in droplets during gelation. We have recently shown that fully polymerized microgel particles can be prepared from aqueous PEGDA droplets in a fluorinated oil (Novec 7500) continuous phase by using a nitrogen-purged microfluidic device.[46] These devices depleted oxygen in the PDMS substrate, preventing consumed oxygen from being replenished during photopolymerization. While this provided conditions for polymerization, the conversion of residual oxygen to ROS was above the threshold that could be tolerated by cells, leading to the observed post-encapsulation cell viability of effectively zero. To provide conditions that allow for polymerization, but are also salubrious to encapsulated cells, we have improved the control of oxygen within the microfluidic purging device. The cell encapsulation system presented here consists of a

nitrogen-jacketed microfluidic device (Figure 3A) with a prepurge channel for the oil phase, in which the oil phase was purged with nitrogen, thus, driving oxygen from the oil before converging with the aqueous phase. All fluid channels were purged with nitrogen jackets to reduce the oxygen solubility in Novec 7500 and prepolymer solution. As depicted in the schematic shown in Figure 3B, an increase in the partial pressure of dissolved nitrogen in the oil phase decreases the oxygen solubility, thus, leading to an oxygen purge from the oil.

For hydrogel forming solutions with identical compositions and using equal UV light intensity and radiation time, the photopolymerization reaction proceeds at a rate that depends only upon the total amount of oxygen in the system. In lieu of directly measuring residual oxygen, the minimum initiator amount required for full polymerization was used as a parameter to indirectly evaluate the remaining oxygen in system. To establish the threshold at which PEGDA microgel particles could be fully polymerized, the initiator concentration was increased until it was sufficient to counterbalance the amount of residual oxygen at a given nitrogen purge pressure. Photopolymerization was conducted in the two-layer nitrogen-jacketed PDMS device, and products were collected at the outlet to examine the extent of polymerization. Results show that less initiator was required to achieve fully photopolymerization as the nitrogen pressure was increased (Figure 4A), confirming that more oxygen is purged at elevated nitrogen pressures. The composition of the hydrogel forming solution was maintained at that used for previous cell encapsulation experiments except for the LAP concentration, which was varied. Cell encapsulation experiments were conducted using the same hydrogel forming solution compositions with a constant nitrogen pressure (P_{N_2} = 7 psi). Under a constant nitrogen purge pressure, the oxygen concentration in the emulsion reaches an equilibrium level, and the reaction rate for the formation of peroxy radicals increases with initiator concentration in the prepolymer solution. Correspondingly, as more peroxy radicals are generated during the polymerization reaction, encapsulated cells sustain more damage. This has been confirmed by the experiment results (Figure 4B), in which the post-encapsulation cell viability decreased from 95.6% to 0.62% as the LAP concentration increased from 0.1 to 0.7 wt %. Employing this system makes it possible to reduce both residual oxygen and initiator required for polymerization, thus reducing the cumulative amount of peroxy radical produced during the polymerization. This is confirmed by Figure 4C, which shows high post-encapsulation viability, 95.6%, for cells encapsulated using this system.

3.4. Prediction of the Peroxy Radical Concentration Using COMSOL

Using the developed reaction-diffusion model and minimum LAP concentrations required to achieve polymerization, the oxygen concentration in the emulsion system was evaluated for each nitrogen pressure. The cumulative peroxy radical amount produced during photopolymerization was also calculated using this model (Figure 5A), and the cumulative effects of peroxy radical generation on cell viability was analyzed (Figure 5B). Compared with experimental results shown in Figure 4B, these modeling results suggest a strong, nonlinear correlation between oxygen radical accumulation and cell viability. The close agreement between the shape of the cell viability curves when plotted as functions of nitrogen pressure and peroxy radical generation conclusively and quantitatively suggest that the decrease in viability is directly related to ROS. These results also explain the observed

collapse of viability in bulk control experiments summarized in Figure 2, and clearly indicate that this effect can be completely mitigated with the use of a nitrogen jacketed microfluidic channel.

4. CONCLUSIONS

In this study, we have introduced and examined a nitrogen microjacketed microfluidic platform to locally control the oxygen concentration in microfluidic channels by varying nitrogen prepurge time and pressure. In this oxygen-controlled microfluidic device, cell-laden droplets with diameters of approximately 40 μm were generated and photopolymerized. The viability of encapsulated cells was evaluated as a function of residual oxygen in the emulsion system, which was ascertained from the minimum initiator concentration required to achieve complete droplet photopolymerization. To elucidate the relationship between reaction inhibition and cell viability, we have modeled the cumulative peroxy radical generation under a constant oxygen concentration with different initiator concentrations using a reaction-diffusion finite element model. The amount of residual oxygen, and therefore the viability of encapsulated cells, was found to be strongly sensitive to nitrogen purge pressure. These results indicate that during oxygen-inhibited photopolymerization, peroxy radicals are produced with a direct and significantly deleterious effect upon post-encapsulation cell viability. At higher nitrogen pressures and ample prepurging times, however, cell viability can be completely recovered.

Supplementary Material

Refer to Web version on PubMed Central for supplementary material.

ACKNOWLEDGMENTS

This work was supported by the National Science Foundation Faculty Early Career Development (CAREER) Program (BBBE 1254608) and the NIH-funded Wyoming IDeA Networks of Biomedical Research Excellence Program (P20RR016474 and P20GM103432). The content is solely the responsibility of the authors and does not necessarily represent the official views of the National Institutes of Health.

REFERENCES

(1). Chang TM Science 1964, 146, 524. [PubMed: 14190240]

(2). Peppas NA; Hilt JZ; Khademhosseini A; Langer R Adv. Mater. 2006, 18 (11), 1345–1360.

(3). Drukker M; Katz G; Urbach A; Schuldiner M; Markel G; Itskovitz-Eldor J; Reubinoff B; Mandelboim O; Benvenisty N Proc. Natl. Acad. Sci. U. S. A. 2002, 99 (15), 9864–9869. [PubMed: 12114532]

(4). Jain K; Asina S; Yang H; Blount ED; Smith BH; Diehl CH; Rubin AL Transplantation 1999, 68 (11), 1693–1700. [PubMed: 10609945]

(5). Kaigler D; Krebsbach PH; Wang Z; West ER; Horger K; Mooney DJ J. Dent. Res. 2006, 85 (7), 633–637. [PubMed: 16798864]

(6). Betz MW; Modi PC; Caccamese JF; Coletti DP; Sauk JJ; Fisher JPJ Biomed. Mater. Res., Part A 2008, 86 (3), 662–670.

(7). Chung C; Mesa J; Miller GJ; Randolph MA; Gill TJ; Burdick JA Tissue Eng. 2006, 12 (9), 2665–2673. [PubMed: 16995800]

(8). Ferreira LS; Gerecht S; Fuller J; Shieh HF; Vunjak-Novakovic G; Langer R Biomaterials 2007, 28 (17), 2706–2717. [PubMed: 17346788]

(9). Lacy PE; Davie JM Annu. Rev. Immunol. 1984, 2 (1), 183–198. [PubMed: 6443340]
(10). Toh WS; Lee EH; Guo X-M; Chan JKY; Yeow CH; Choo AB; Cao T Biomaterials 2010, 31 (27), 6968–6980. [PubMed: 20619789]
(11). Weber LM; He J; Bradley B; Haskins K; Anseth KS Acta Biomater. 2006, 2 (1), 1–8. [PubMed: 16701853]
(12). Baroli BJ Chem. Technol. Biotechnol. 2006, 81 (4), 491–499.
(13). Hwang DK; Oakey J; Toner M; Arthur JA; Anseth KS; Lee S; Zeiger A; Van Vliet KJ; Doyle PS J. Am. Chem. Soc. 2009, 131 (12), 4499–4504. [PubMed: 19215127]
(14). Dendukuri D; Gu SS; Pregibon DC; Hatton TA; Doyle PS Lab Chip 2007, 7 (7), 818–828. [PubMed: 17593999]
(15). Nie Z; Xu S; Seo M; Lewis PC; Kumacheva EJ Am. Chem. Soc. 2005, 127 (22), 8058–8063.
(16). Seiffert S; Weitz DA Polymer 2010, 51 (25), 5883–5889.
(17). Griffin DR; Weaver WM; Scumpia PO; Di Carlo D; Segura T Nat. Mater. 2015, 14 (7), 1–8. [PubMed: 25515988]
(18). Burdick JA; Khademhosseini A; Langer R Langmuir 2004, 20 (13), 5153–5156. [PubMed: 15986641]
(19). Peyton SR; Raub CB; Keschrumrus VP; Putnam A Biomaterials 2006, 27 (28), 4881–4893. [PubMed: 16762407]
(20). Tibbitt MW; Rodell CB; Burdick JA; Anseth KS Proc. Natl. Acad. Sci. U. S. A. 2015, 112 (47), 14444–14451. [PubMed: 26598696]
(21). Khademhosseini A; Langer R Biomaterials 2007, 28 (34), 5087–5092. [PubMed: 17707502]
(22). Kang A; Park J; Ju J; Jeong GS; Lee S-H Biomaterials 2014, 35 (9), 2651–2663. [PubMed: 24439405]
(23). Vos PD; Andersson A; Tam SK; Faas MM; Halle JP Immunol., Endocr. Metab. Agents Med. Chem. 2006, 6 (2), 139–153.
(24). Gift EA; Weaver JC Cytometry 2000, 39 (4), 243–249. [PubMed: 10738276]
(25). Lin C-C; Anseth KS Proc. Natl. Acad. Sci. U. S. A. 2011, 108 (16), 6380–6385. [PubMed: 21464290]
(26). Li CY; Wood DK; Huang JH; Bhatia SN Lab Chip 2013, 13 (10), 1969–1978. [PubMed: 23563587]
(27). Du Y; Lo E; Ali S; Khademhosseini A Proc. Natl. Acad. Sci. U. S. A. 2008, 105 (28), 9522–9527. [PubMed: 18599452]
(28). Panda P; Ali S; Lo E; Chung BG; Hatton TA; Khademhosseini A; Doyle PS Lab Chip 2008, 8 (7), 1056–1061. [PubMed: 18584079]
(29). Kloxin AM; Tibbitt MW; Anseth KS Nat. Protoc. 2010, 5 (12), 1867–1887. [PubMed: 21127482]
(30). Haghgooie R; Toner M; Doyle PS Macromol. Rapid Commun. 2009, 31 (2), 128–134. [PubMed: 21590884]
(31). Anna SL; Bontoux N; Stone HA Appl. Phys. Lett. 2003, 82 (3), 364.
(32). Thorsen T; Roberts RW; Arnold FH; Quake SR Phys. Rev. Lett. 2001, 86 (18), 4163–4166. [PubMed: 11328121]
(33). Utada AS; Lorenceau E; Link DR; Kaplan PD Science 2005, 308 (5721), 537–541. [PubMed: 15845850]
(34). Luo D; Pullela SR; Marquez M; Cheng Z Biomicrofluidics 2007, 1 (3), 034102–034106.
(35). Li CY; Wood DK; Hsu CM; Bhatia SN Lab Chip 2011, 11 (17), 2967–2975. [PubMed: 21776518]
(36). O'Brien AK; Bowman CN Macromol. Theory Simul. 2006, 15 (2), 176–182.
(37). O'Brien AK; Bowman CN Macromolecules 2006, 39 (7), 2501–2506.
(38). Duffy DC; McDonald JC; Schueller OJA; Whitesides GM Anal. Chem. 1998, 70 (23), 4974–4984. [PubMed: 21644679]
(39). Tang MD; Golden AP; Tien JJ Am. Chem. Soc. 2003, 125 (43), 12988–12989.
(40). Esterbauer H; Gebicki J; Puhl H; Jürgens G. Free Radical Biol. Med. 1992, 13 (4), 341–390. [PubMed: 1398217]

(41). Stadtman ER; Levine RL Amino Acids 2003, 25 (3–4), 207–218. [PubMed: 14661084]
(42). Brooker RJ Genetics: Analysis and Principles; Addison-Wesley, 1999.
(43). Whittemore ER; Loo DT; Watt JA; Cotmans CW Neuroscience 1995, 67 (4), 921–932. [PubMed: 7675214]
(44). Armstrong D; Browne R Free Radicals Biol. Med. 1994, 366, 43–58.
(45). Imlay JA; Linn S Science 1988, 240 (4857), 1302–1309. [PubMed: 3287616]
(46). Krutkramelis K; Xia B; Oakey J Lab Chip 2016, 16 (8), 1457–1465. [PubMed: 26987384]
(47). Clarson SJ; Semlyen JA Siloxane Polymers; Prentice-Hall: Englewood Cliffs, NJ, 1993.
(48). Weber LM; Hayda KN Tissue Eng., Part A 2008, 14 (12), 1959–1968. [PubMed: 18724831]
(49). Fairbanks BD; Schwartz MP; Bowman CN; Anseth KS Biomaterials 2009, 30 (35), 6702–6707. [PubMed: 19783300]
(50). Maillard B; Ingold KU; Scaiano JC J. Am. Chem. Soc. 1983, 105 (15), 5095–5099.
(51). Bamford CH; Dewar M Proc. R. Soc. London, Ser. A 1949, 198 (1053), 252–267.
(52). Mayo FR Acc. Chem. Res. 1968, 1 (7), 193–201.
(53). Ladygin BY; Zimina GM; Vannikov AV High Energy Chem. 1984, 18 (4), 241–244.
(54). Smaller B; Remko JR; Avery EC J. Chem. Phys. 1968, 48 (11), 5174–5181.
(55). Binks BP; Whitby CP Colloids Surf., A 2005, 253 (1–3), 105–115.
(56). Edd JF; Di Carlo D; Humphry KJ; Köster S.; Irimia D; Toner M.; Weitz DA Lab Chip 2008, 8 (8), 1262–1264. [PubMed: 18651066]
(57). Lagus TP; Edd JF J. Visualized Exp. 2012, 64, 4096–4096.
(58). Du Y; Lo E; Vidula MK; Khabiry M; Khademhosseini A Cell. Mol. Bioeng. 2008, 1 (2–3), 157–162. [PubMed: 19953195]
(59). Clausell-Tormos J; Lieber D; Baret J-C; El-Harrak A; Miller OJ; Frenz L; Blouwolff J; Humphry KJ; Köster S; Duan H Chem. Biol. 2008, 15 (5), 427–437. [PubMed: 18482695]
(60). Riess JG; Le Blanc M Pure Appl. Chem. 1982, 54 (12), 2383–2406.
(61). Mü A; Jovalekic M; Tenbohlen S Solubility study of different gases in mineral and ester-based transformer oils. 2012 International Conference on Condition Monitoring and Diagnosis (CMD), Bali, 23–27 Sept., 2012, IEEE, 2012, pp 937–940; DOI: 10.1109/CMD.2012.6416307.
(62). Decker C; Jenkins AD Macromolecules 1985, 18 (6), 1241–1244.
(63). Minoura N; Tani S; Nakagawa TJ Appl. Polym. Sci. 1978, 22 (3), 833–836.
(64). Allen SM; Fujii M; Stannett V; Hopfenberg HB J. Membr. Sci. 1977, 2, 153–163.

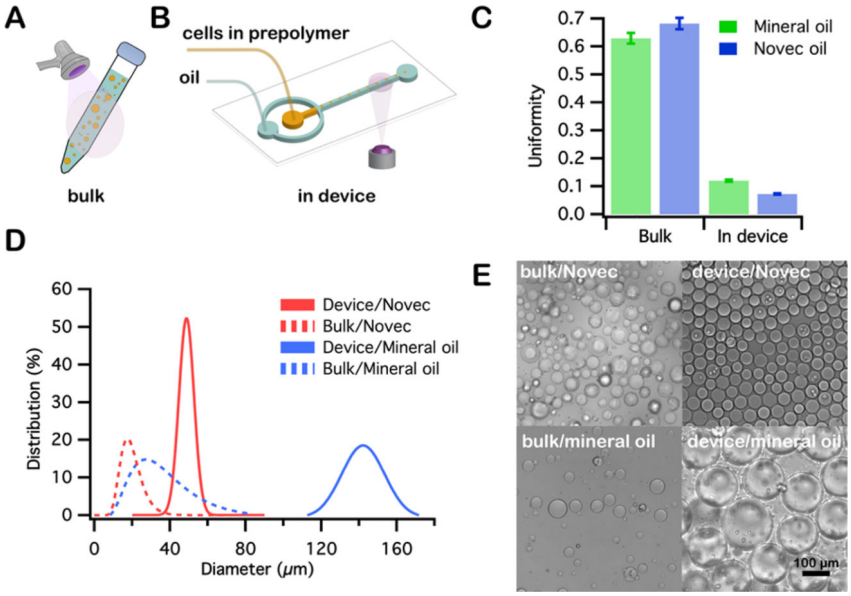

Figure 1.

Cell encapsulation in bulk (A) and in a cross-flow microfluidic channel (B). Uniformity (C) and size distribution (D) of hydrogel microparticles produced using different polymerization methods. (E) Images of microparticles obtained through different methods and oil phases: in bulk and in device using Novec 7500 and mineral oil.

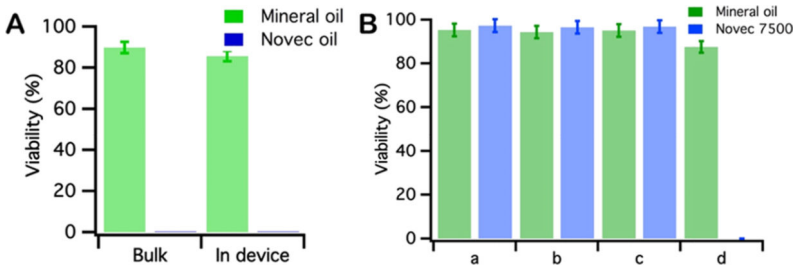

Figure 2.

(A) Post-encapsulation viability of cells encapsulated and polymerized via bulk and microfluidic processing, using mineral oil and Novec 7500, respectively. (B) Cell viability following processing in microfluidic droplets as a function of different processing conditions and aqueous phase formulations. All experiments were repeated using both mineral oil and Novec 7500 as the carrier phase. Droplets contained (a) cells in PBS, (b) cells in 10% PEGDA, (c) cells in 10% PEGDA exposed to UV light, and (d) cells in 10% PEGDA plus 1 wt % LAP exposed to UV light.

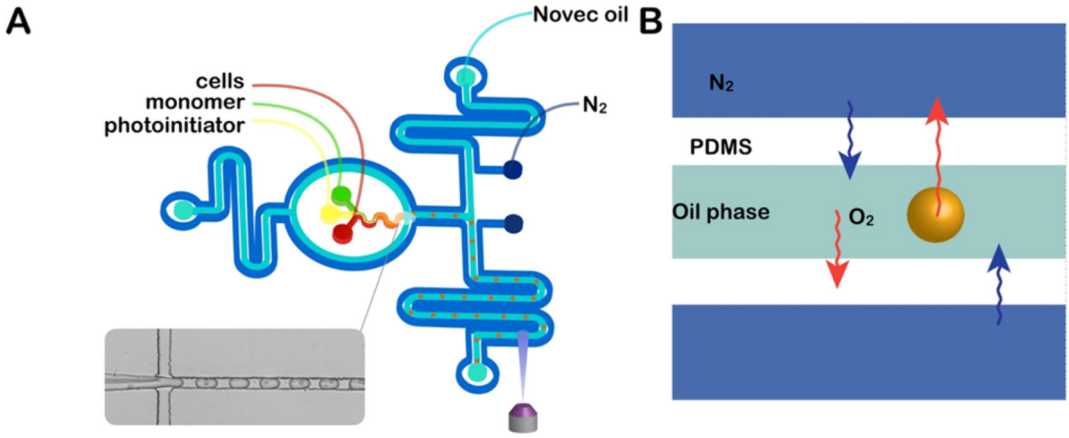

Figure 3.

Cell encapsulation using a nitrogen jacketed two-layer microfluidic device. (A) Schematic illustration of the two-layer nitrogen jacketed microfluidic device. The initiator, cell suspension, and monomer mixture were individually introduced and fully mixed in device and merged with a fluorocarbon oil to generate cell-laden droplets at the nozzle of the first layer of the device. Fluid flow channels are bounded on each side by in-plane nitrogen channels. Formed emulsion droplets were photopolymerized to hydrogel by exposure to UV light in the second layer of the device. (B) Schematic of oxygen purging from the system. Increased nitrogen pressure decreases oxygen solubility, which results in oxygen diffusion from the droplet and oil into the PDMS matrix.

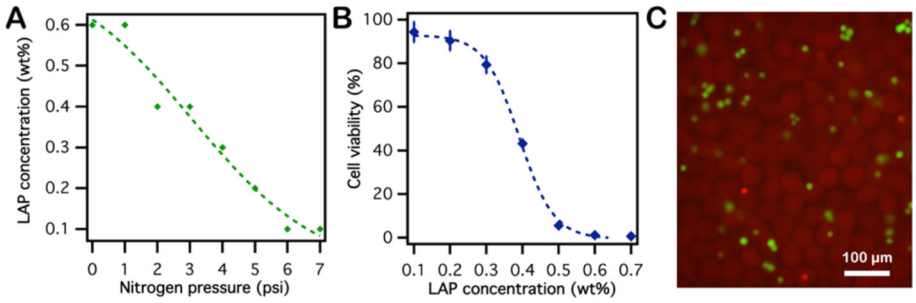

Figure 4.

(A) Minimum LAP concentration required to achieve full photopolymerization under different nitrogen pressures. As the nitrogen purge pressure is increased, the residual oxygen in the system decreasing, thus requiring decreased photoinitiator concentrations for full polymerization. (B) Post-encapsulation viability of cells with different LAP concentration at a constant nitrogen pressure (PN_2 = 7 psi) in the nitrogen prepurged microfluidic device. (C) Post-encapsulation viability of cells was assayed by live–dead stain (live cells are green, dead cells are red).

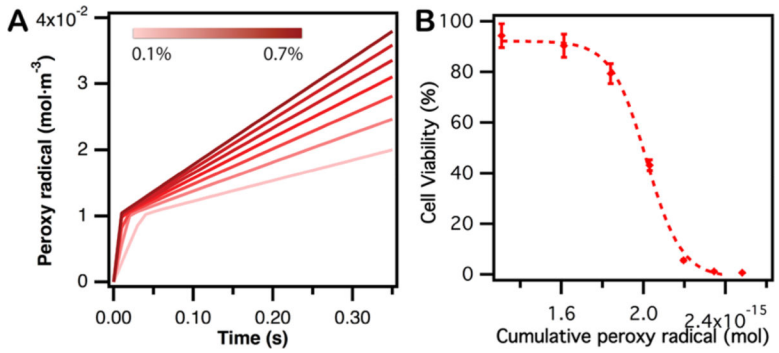

Figure 5.

(A) Cumulative concentration of peroxy radicals as a function of UV radiation time in the droplets or hydrogel micro particles. The photoinitiator concentration was varied from 0.1 to 0.7 wt %. (B) Post-encapsulation viability of cells in hydrogel micro particles following photopolymerization for 0.35 s. The cumulative peroxy radical generation maps to the photoinitiator concentration required for complete photopolymerization (Figure 4B) and is a function of residual oxygen in the emulsion.